# Sensitivity of the African and Asian Monsoons to Mid-Holocene Insolation and Data-Inferred Surface Changes

DELPHINE TEXIER,* NATHALIE DE NOBLET, AND PASCALE BRACONNOT

*Laboratoire des Sciences du Climat et de l'Environnement/DSM, Unité Mixte de Recherche CEA-CNRS, Gif-sur-Yvette, France*

(Manuscript received 8 July 1998, in final form 26 February 1999)

ABSTRACT

Orbital forcing alone is not sufficient to explain the massive northward penetration of monsoon rains in Africa shown by data during the mid-Holocene (6000 yr ago). Feedbacks associated with changes in SSTs and land surface cover may be necessary to produce a sufficient increase in the monsoon. A step toward a better understanding of the respective role of oceans and land surfaces is to design sensitivity studies with prescribed forcings, inferred from observations. In the first study, SSTs are lowered in the upwelling regions offshore of West Africa and Somalia, and increased in the Bay of Bengal and South China Sea. In the second simulation, the modern Sahara desert is replaced by a combination of xerophytic woods/scrub and grassland.

In both cases the amount of water vapor advected from oceanic sources is increased north of 10°N in Africa in response to the increased land–sea temperature contrast, thereby enhancing rainfall. But the magnitude of the simulated changes is much larger when land surface is modified. The lower albedo (compared to desert) increases the amount of radiation absorbed by the surface in northern Africa and warms it up, and the larger roughness length increases both the sensible and latent heat fluxes. Moreover, vegetation is more efficient in recycling water than a bare soil, and the release of latent heat in the atmosphere increases convection, which in turn helps maintain the onshore oceanic advection. The monsoon season is then lengthened by 1–2 months compared to all other simulations reported in the paper.

The intensity of monsoon rains is also modified in Asia in both sensitivity experiments. Warmer SSTs in the Bay of Bengal and South China Sea reduce the land–sea contrast and therefore the inland penetration of monsoon rains. Changes in the position of the main large-scale convergence area in the case of a green Sahara enhances the precipitation in India.

Changes are also discussed in terms of atmospheric circulation. For example, the tropical easterly jet at 200 hPa is increased in all 6-kyr-BP simulations, but only over Africa in the case of a prescribed green Sahara. The African easterly jet has been pushed at higher altitude in response to all prescribed forcings; wind speed is then reduced at 700 hPa but increased at higher altitude.

## 1. Introduction

During the mid-Holocene (6 kyr BP), northern Africa, Arabia, and southern Asia experienced conditions much wetter than today. Lakes and moisture-demanding vegetation types occurred in now-arid regions (Street and Grove 1976; van Campo et al. 1982; Swain et al. 1983; Petit-Maire and Page 1992; Street-Perrott and Perrott 1993; Jarvis 1993; Roberts et al. 1993; Winkler and Wang 1993; Jolly et al. 1998; Yu et al. 1998). These wetter conditions have been interpreted as resulting from the intensification and the northward expansion of the Afro–Asian monsoon, induced by a 5% increased summer incoming solar radiation (insolation) at the top of the atmosphere (COHMAP 1988). This interpretation is also supported by oceanic data. For instance, changes in the composition of planktonic foraminifera in sediment cores from the Arabian Sea have been related to an intensification of the summer upwelling, resulting from the strengthening of the southwest Asian monsoon winds (Prell 1984a,b; Prell and van Campo 1986). Moreover changes in the $^{18}O/^{16}O$ ratios of planktonic foraminifera indicate a decreased salinity in the Bay of Bengal, attributed to an increase of freshwater input of the Ganges–Brahmaputra and Irrawaddy rivers (Duplessy 1982).

A first attempt to explain mid-Holocene environmental changes has consisted in forcing atmospheric general circulation models (AGCMs) with the 6-kyr-BP insolation change while the surface characteristics, such as

* Current affiliation: Department of Meteorology, University of Reading, Reading, United Kingdom.

*Corresponding author address:* Dr. Nathalie de Noblet, Laboratoire des Sciences du Climat et de l'Environnement/DSM, Unité Mixte de Recherche CEA-CNRS, Bâtiment 709/Orme des Merisiers, 91191 Gif-sur-Yvette Cedex, France.
E-mail: noblet@lsce.saclay.cea.fr

TABLE 1. Boundary conditions used for the experiments.

| Name of expt: Time period | Boundary conditions | | | |
|---|---|---|---|---|
| | Orbital parameters | $CO_2$ | SST | Vegetation |
| Ctrl: Present day | Modern<br>eccentricity: 0.016724<br>obliquity: 23.446<br>precession: 102.24 | 345 ppmv | Modern | Modern |
| OF: 6 kyr BP | 6 kyr BP<br>eccentricity: 0.018682<br>obliquity: 24.105<br>precession: 0.87<br>(Berger 1978) | 280 ppmv<br>(Raynaud et al. 1993) | Modern | Modern |
| OFSST: 6 kyr BP | 6 kyr BP | 280 ppmv | Modern + SST changes | Modern |
| OFGS: 6 kyr BP | 6 kyr BP | 280 ppmv | Modern | Modern + green Sahara |

vegetation distribution or sea surface temperatures (SSTs), were kept as modern (Kutzbach and Guetter 1986; COHMAP 1988; Kutzbach et al. 1993; Liao et al. 1994; de Noblet et al. 1996a; Hewitt and Mitchell 1996; Hall and Valdes 1997; Masson and Joussaume 1997). These studies have shown that the 6-kyr-BP insolation change generated stronger-than-present African and Asian summer monsoons. However, comparisons with palaeoenvironmental data over northern Africa have pointed out that the magnitude of monsoon changes was underestimated by models (Yu and Harrison 1996; Texier et al. 1997; Joussaume et al. 1999). These results suggest that the 6-kyr-BP orbital change alone is not sufficient to produce the observed climate change; internal feedbacks must then be accounted for.

Numerical experiments have shown that African and Asian summer monsoons, at present as well as during the mid-Holocene, are sensitive to modifications in the land surface consequent to changes in 1) vegetation (e.g. Xue and Shukla 1993, 1996; Sud et al. 1988; Street-Perrott et al. 1990; Kutzbach et al. 1996; Claussen and Gayler 1997; Texier et al. 1997) and 2) lakes and wetlands (Coe and Bonan 1997; Bröstrom et al. 1998). The prescription of vegetation in the Sahara 6000 yr ago, for example, allows the monsoon to penetrate farther north.

Changes in the prescription of SSTs may also have significant effect on the African and Asian monsoons as discussed, for example, for present-day climate, by Palmer (1986), Lamb and Peppler (1992), and Semazzi et al. (1996). Regional changes in SSTs have been reconstructed for the early to mid-Holocene in the Atlantic, Pacific, and Indian Oceans, as well as in the Mediterranean Sea (Ruddiman and Mix 1993; Morley and Dworetzky 1993; Prell and Marvil 1990; Schulz 1995; Kallel et al. 1997). Contrary to what has been done for land surfaces, no attention has been paid so far to the effects of mid-Holocene SST-prescribed changes (inferred from sea-core analysis) on the northern tropical monsoons. The only experiments reported in the literature refer to the coupling with an oceanic model (Kutzbach and Liu 1997; Hewitt and Mitchell 1998). Moreover, quantifying and comparing the respective role of changing land and ocean surfaces on both the Asian and African monsoons for this period, using the same AGCM, has not yet been done. This is what we propose to do in this study. The surface changes that we prescribe are derived from proxy data. They may be exaggerated given the scarcity of data and the size of the model grid cells (see section 2b), but they do not exceed the error bars of the reconstructions. We will mainly focus on the summer monsoon response since it is the prominant signal. The model used and the definition of the experiments are presented in section 2. All simulated climates are described in section 3 and compared (in terms of the mechanisms of the simulated changes) in section 4, before the conclusions (section 5).

## 2. Description of the experimental set

Four simulations (Table 1) were carried out to distinguish the respective roles of orbital forcing, and ocean and land-surface changes. Orbital parameters and atmospheric $CO_2$ concentration for the control and all 6-kyr-BP experiments were defined following the Palaeoclimate Modelling Intercomparison Project (PMIP; Joussaume and Taylor 1995). Sea surface temperature for the control (Ctrl), orbital forcing (OF), and OFGS are taken from Reynolds (1988). The vegetation distribution used in Ctrl, OF and OFSST is potential and prescribed from Prentice et al. (1992).

In OFSST a mid-Holocene anomaly inferred from sea-core analysis [see section 2b(2)] is added to the control sea surface temperature. In OFGS the present Sahara is replaced by a combination of warm grasses and xerophytic woods/scrub [see section 2b(3)]. Differences between OF and Ctrl show the impact of changes in orbital forcing and $CO_2$ concentration on the simulated climate and can be compared to the results obtained within PMIP. Differences between OFSST and OF quantify the sensitivity of the simulated mid-Holocene climate to changes in sea surface temperatures. Differences between OFGS and OF quantify the sensitivity of the simulated mid-Holocene climate to changes in vegetation in the Sahara.

### a. The atmospheric general circulation model

Experiments have been run with version 5.3 of the LMD AGCM (Sadourny and Laval 1984; Harzallah and Sadourny 1995), which has also been used by Masson and Joussaume (1997) to run the standard PMIP simulation. The LMD AGCM is a gridpoint model that has 64 points regularly spaced in longitude (equivalent to 5.625°) and 50 points regularly spaced in the sine of latitude (equivalent to ~2° in equatorial regions). The atmosphere is divided into 11 vertical sigma levels, unevenly spaced, including 4 levels in the planetary boundary layer, 4 in the free troposphere, and 3 in the stratosphere. The model is run with full seasonal cycle but no diurnal cycle for insolation. The solar radiation scheme is the algorithm of Fouquart and Bonnel (1980); the longwave radiation scheme is from Morcrette (1991). Three condensation schemes are used in a sequential mode: large-scale condensation, moist-adiabatic adjustment (Manabe and Strickler 1964), and deep convection (Kuo 1965). The LMD5.3 AGCM incorporates a modified version of the Schématisation des Echanges Hydriques à l'Interface entre la Biosphère et l'Atmosphère land-surface scheme (Ducoudré et al. 1993). These modifications have been performed in the scope of previous studies (de Noblet et al. 1996b; Texier et al. 1997) for which the LMD5.3 AGCM had been coupled to the BIOME1 model of Prentice et al (1992).

All experiments are 16 yr long and monthly means are made for the last 15 yr. Student's t-tests have been performed to assess the significance of the simulated changes. We then only discuss here the changes that are statistically significant.

### b. Boundary conditions

#### 1) Changes in insolation prescribed for the mid-Holocene climate

The 6-kyr-BP period is characterized by an enhanced seasonal cycle of insolation (compared to today) in the Northern Hemisphere (NH). On average over the NH about 5% more incoming solar radiation was received during summer and 5% less during winter. This increased seasonal contrast mainly resulted from the orbital precession of the equinoxes. At present the winter solstice occurs when the earth is at perihelion and the summer solstice when it is at aphelion. Six-thousand years ago, the position of solstices and equinoxes, relative to perihelion, were rotated by about 90° (Table 1). Consequently, the earth was more distant from the Sun during the NH winter and closer during the NH summer. An increased obliquity at 6 kyr BP induced an additional increase of the seasonal cycle of insolation, mostly at high northern latitudes. The slight increase in eccentricity had minor impacts.

Insolation changes follow PMIP recommendations (Joussaume and Taylor 1995). Orbital parameters and insolation have been computed following Berger (1978), and in all experiments the vernal equinox was set to 1200 LT 21 March. Having fixed this date, the maximum increase between 6 kyr BP and present occurred from May to September in the northern Tropics (Fig. 1).

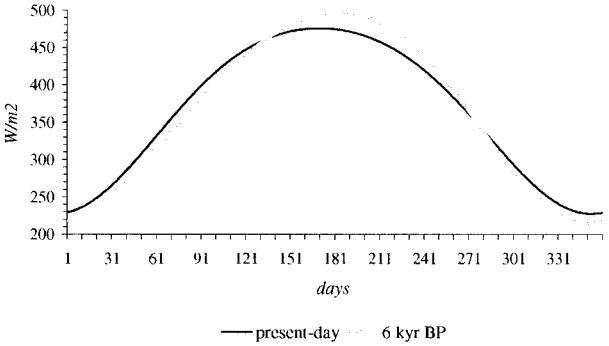


FIG. 1. Daily insolation at 30°N for present day (black line) and mid-Holocene (6 kyr BP, gray line) for a 360-day-long year.

The 6-kyr-BP monthly means (averaged over 15 yr of simulation) have been computed using the present-day calendar rather than a more appropriate definition of months based on celestial longitude (Kutzbach and Gallimore 1988; Joussaume and Braconnot 1997). Since our orbitally induced experiment is a PMIP simulation, we followed the recommendations of this project to keep the possible comparison with its results.

#### 2) Changes in SST prescribed for the mid-Holocene climate

Cadet and Houston (1984) have shown that the main sources of water vapor for the African monsoon are located in the tropical Atlantic and the Gulf of Guinea. In the same way, water vapor for the Asian monsoon is provided by the Indian Ocean and the Arabian Sea (Cadet and Reverdin 1981). AGCM simulations carried out by Druyan and Koster (1989) for the Sahelian climate, and by Joussaume et al. (1986) for the climates of the globe, show that the models are capable of reproducing this aspect of the real world. Given that we were mainly concerned with changes in tropical monsoons, we have restricted, in our simulations, the prescribed changes in SSTs in the eastern tropical Atlantic (including the Gulf of Guinea) and in the Indian Ocean, drawing on observations from Ruddiman and Mix (1993), Morley and Dworetzki (1993), and Schulz (1995). We also included changes in the Mediterranean Sea from N. Kallel (1997, personal communication). Changes in the Mediterranean are unlikely to influence the intensity of the summer monsoon in Africa, but could influence the inflow of moisture in northern Africa through changes in the winter circulation (not discussed in this paper).

Observations show considerable variability in the values of SST changes for the mid-Holocene period: in each of the documented basins, both positive and neg-

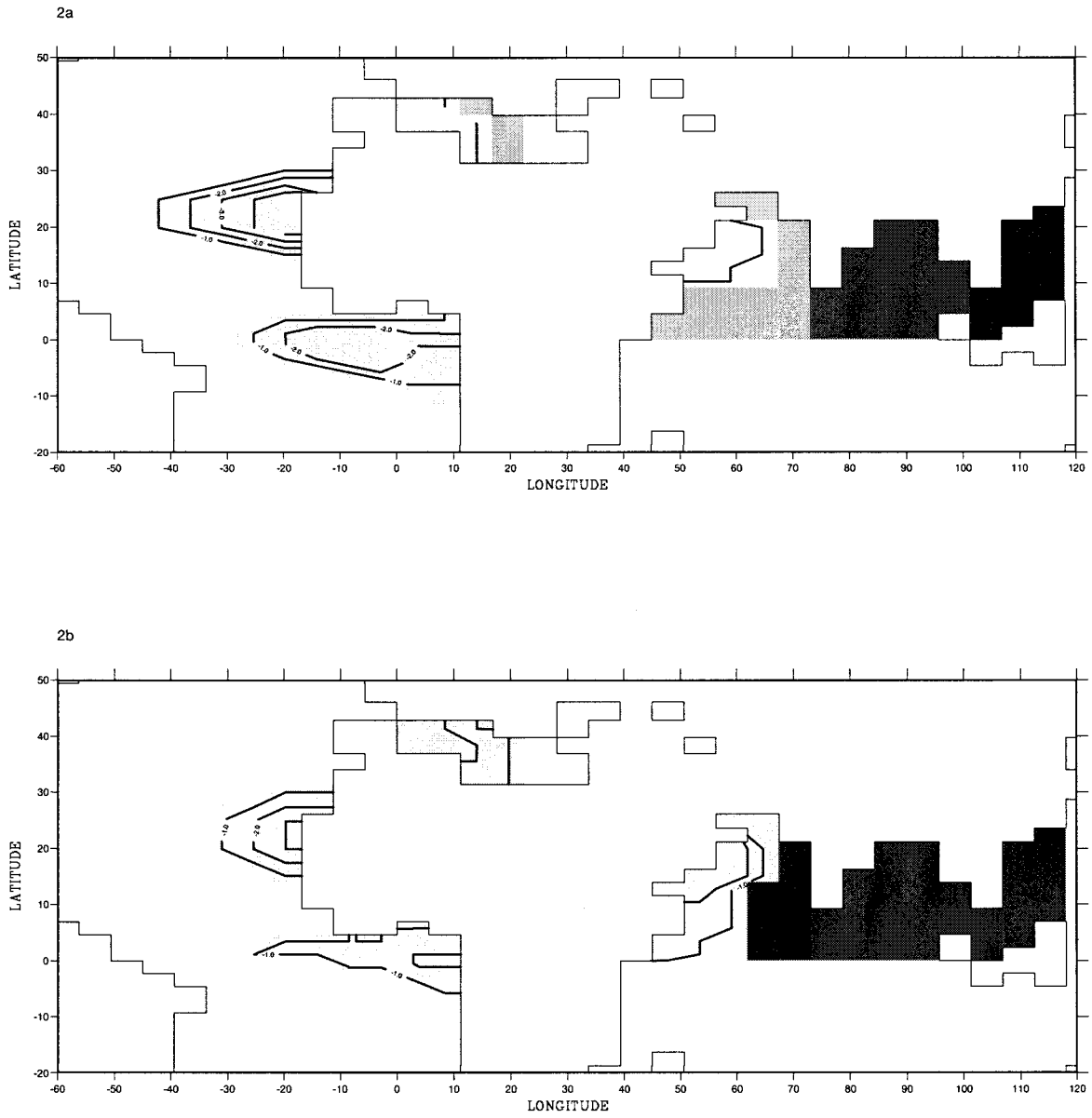


FIG. 2. Prescribed changes in SSTs (°C) for the mid-Holocene, for months of (a) Feb and (b) Aug. Isolines are −1°, −2°, −3°, and −4°C. Shading from the lightest to the darkest are for differences 1) lower than −0.5°C, 2) from −0.5° to 0°C, 3) from 0° to 0.5°C, and 4) larger than 0.5°C.

ative anomalies exist. In order to extract a dominant signal from a large enough number of points, means have been computed based on data for the whole Holocene period (9000–6000 yr BP). In this way the general picture that one gets for the mid-Holocene is a moderate to strong cooling in the Atlantic, Mediterranean, and Arabian regions, contrasting with a slight to moderate warming farther east in the Bay of Bengal and South China Sea. The change in SST that we have prescribed for the months of February (August) is (Fig. 2) −5°C (−3°C) off western Sahara; −2°C (−2°C) in the Gulf of Guinea; −3°C (−1°C) east of the Gulf of Guinea, −1°C (−3°C) in the western Mediterranean Sea; −1°C (−3°C) in the Arabian Sea; −1°C (+1°C) in the east Oman Sea; +0.5°C (+0.5°C) in the Bay of Bengal; and +1.5°C (+0.5°C) in the South China Sea. To avoid sharp discontinuities in the SSTs, anomalies have been smoothed out at the boundaries of the documented basins. Consequently, the surface of the latter may be overestimated, but we would like to point out that our simulation is a sensitivity study rather than an attempt to make a realistic experiment. Finally, a sinusoidal time interpolation was then carried out to yield a daily distribution of SST change from 1 January to 31 December. This anomaly field was added to the present-day distribution used to force the control simulation.

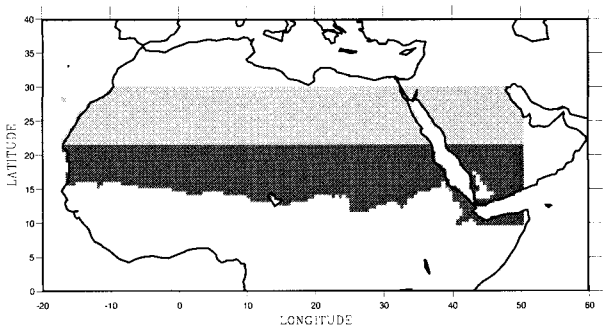


FIG. 3. Prescribed changes in the vegetation distribution for the mid-Holocene climate. Dark gray indicates that desert was replaced by xerophytic woods/scrub, and light gray indicates that desert was replaced by warm grassland.

#### 3) CHANGES IN VEGETATION PRESCRIBED FOR THE MID-HOLOCENE CLIMATE

According to Jolly et al. (1998) vegetation was present in most of the Sahara at 6 kyr BP. They found evidences of warm grasses north of 20°N (up to about 30°N), and of xerophytic woods/scrub farther south (north of Lake Chad). We have then modified our present-day vegetation distribution replacing North African and Arabian hot deserts by a vegetation of xerophytic woods/scrub up to the northern Tropic and of warm grass/shrub from the northern Tropic up to 30°N (Fig. 3). Although this partition is inferred from a pollen-derived biome distribution, it may overestimate the 6-kyr-BP vegetation development. Indeed, if settlements of vegetation have been found in many places between the present-day northern limit of the Sahelian vegetation band and 30°N, nothing indicates that the Sahara was covered by a continuous vegetation rather than by patches. We have chosen, for our sensitivity experiment, to prescribe the largest possible change in vegetation. It is accompanied by a decreased land-surface albedo (from 34% to 21%), an increased roughness length (from 0.02 to 0.16 m), and decreased resistances to evapotranspiration (from more than 600 s $m^{-1}$ in the case of a bare soil to about 150 s $m^{-1}$ when vegetation is present). The albedo of uncovered soil has also been lowered (from 34% to about 26%). It is computed in our land-surface scheme and is always 20% larger than the albedo of the surrounding vegetation. Maximum available water content in the soil is set to 150 mm at all land points and therefore has not been changed in northern Africa.

## 3. Simulated present and 6-kyr-BP climates

### *a. Present-day climate*

The summer monsoon flow, in the model as in the actual world, is an onshore wind driven by a gradient of sea level pressure between colder oceans (high pressure) and warmer continents (low pressure). The flow is represented in Fig. 4 using the transport of latent heat in the boundary layer. Most of the water vapor that is advected over North Africa comes from the Gulf of Guinea, and a smaller contribution comes from the North Atlantic. For the Asian monsoon, water vapor is mainly advected from the Indian Ocean, the Arabian Sea, and the Bay of Bengal.

The broad features of present-day precipitation in North Africa and in Asia during the monsoon season (from June to September, herafter JJAS) are well captured by the model when compared to Legates and Will-

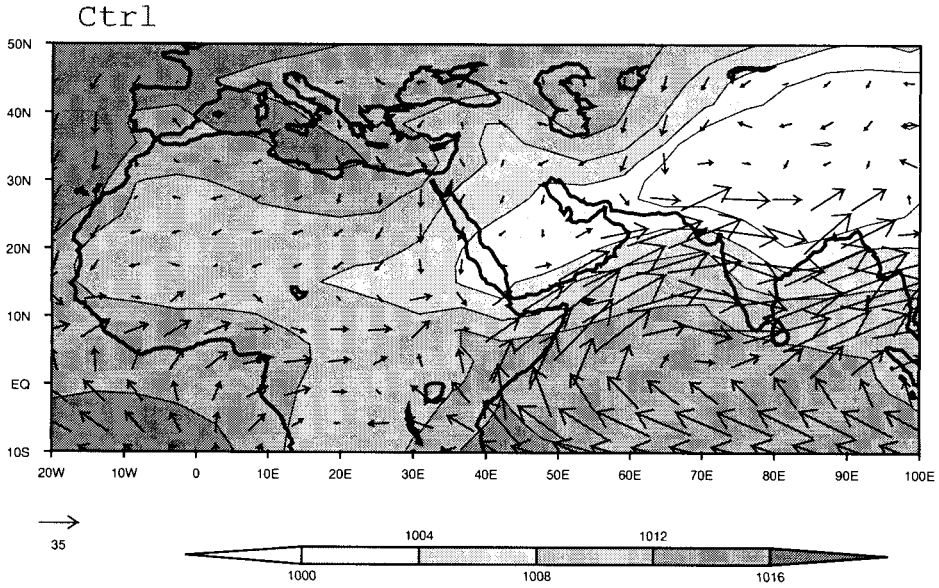


FIG. 4. Transport (vectors) of latent heat ($10^8$ W $m^{-1}$) in the boundary layer in Jun–Sep (JJAS) as simulated by the LMD AGCM for present day (Ctrl). Sea-level pressure (SLP; hPa) is shaded. Isolines are 1000, 1004, 1008, 1012, and 1016 hPa.

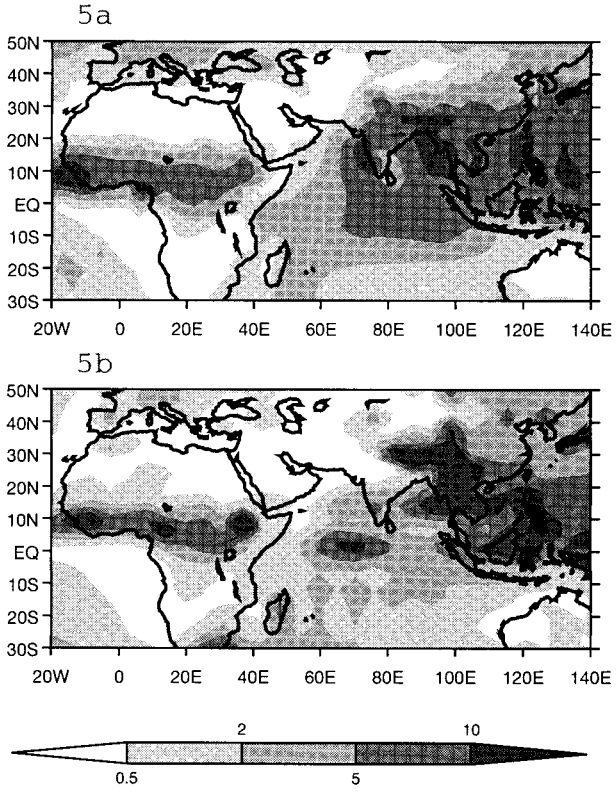


FIG. 5. Mean rainfall (mm day$^{-1}$) averaged over JJAS as (a) observed from Legates and Willmott (1990), and (b) simulated by the LMD AGCM for present day (Ctrl).

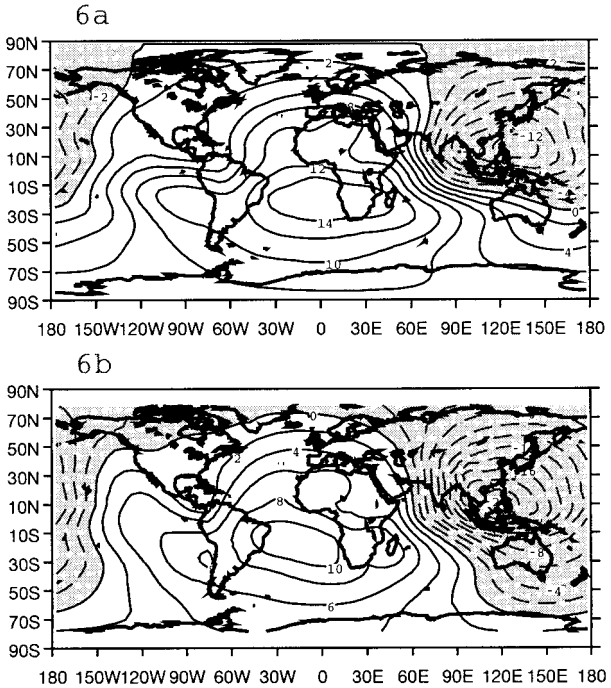


FIG. 6. Mean 200-hPa velocity potential ($\times 10^6$ m$^2$ s$^{-1}$) in JJAS as (a) obtained from 10-yr ECMWF analyses (1979–88; courtesy of the Program for Climate Model Diagnosis and Intercomparison), and (b) simulated by the LMD AGCM for present day (Ctrl). Negative values (i.e., regions with upper-level divergence) are shaded. Isolines are every $2 \times 10^6$ m$^2$ s$^{-1}$. Negative contours are dashed.

mott's (1990) data (Fig. 5). The position of the intertropical convergence zone (i.e., the regions of maximum rainfall rates; ITCZ) in North Africa, for example, is centered around 8°N, as expected, although the rates we simulate are too large (by 2–3 mm day$^{-1}$). North of Lake Chad the model tends to underestimate rainfall (by 1–2 mm day$^{-1}$), and this is due to the early retreat of the monsoon in this model: in August the ITCZ has already started its southward migration while in reality it continues to progress northward until early September. The model produces too much rainfall over the mountainous regions (mainly Ethiopia and the Tibetan Plateau).

In Asia and the northern Indian Ocean the model displays a split ITCZ that is not found in the data, with one maximum located south of the Arabian Sea, and another one in Indochina and the northern Indian Ocean (the southern branch will herafter be referred to as the ''oceanic ITCZ,'' while ''continental ITCZ'' will be employed for the northern branch). We may note though that in the real world there is a bimodal behavior of the ITCZ over Indian longitudes, the oceanic mode being established during breaks in the monsoon. Observations show that, in general, it is the continental rather than the oceanic ITCZ that should be dominant (Gadgil et al. 1992; Ju and Slingo 1995). India is too dry, especially in the north.

If we compare our simulated velocity potential at 200 hPa, which displays the global scale characteristics of the Northern Hemisphere summer monsoon, to 1980–87 European Centre for Medium-Range Weather Forecasts (ECMWF) analyses (Fig. 6a), we can see that the model reproduces correctly the broad features of the large-scale circulation. However the large-scale upper-level divergence (low-level convergence) is overestimated in east Asia–west Pacific, while the convergence (low-level divergence) in south Atlantic–southern Africa (Fig. 6b) is underestimated. The LMD model therefore creates a surface convergence zone in east Asia–west Pacific that is too strong, and that pulls to the east the main low-level flow (including water vapor). This may explain why most of the rainfall associated with the Indio–Asian summer monsoon falls in the eastern part of the area while the west remains too dry (Fig. 5).

### *b. Orbitally induced 6-kyr-BP climate*

The first-order effect of the increased summer insolation 6 kyr BP is to enhance the summer warming of the Northern Hemisphere continents. Differences between OF and Ctrl are larger than 2°C (not shown) and result from a combination of changes in both orbital parameters and atmospheric $CO_2$ concentration. The latter being reduced 6 kyr BP compared to present (280 vs 320 ppm), the climate would have been cooler 6 kyr

ago if insolation had not been changed. The sensitivity to the small change in carbon dioxide is not very large though given that SSTs are prescribed and not computed as in scenarios of future climate change. Moreover, we have carried out simulations (unpublished work) that show that the role of $CO_2$ in such ''PMIP-like'' simulations is minor. We may also point out that the most important climate changes observed (from paleodata) 6 kyr ago result from the change in seasonal contrast, which is not affected by the reduced carbon dioxide.

SSTs being the same in both Ctrl and OF, and northern lands being warmer, the ocean–land temperature and pressure gradients are stronger than present, and the inland penetration of moisture (Fig. 7a) is increased 6 kyr BP. As a result, monsoon rains and the zones of maximum precipitation are extended farther north (Fig. 8a).

In northern Africa, in the northern part of the ITCZ (averaged from 10° to 15°N, 20°W to 40°E, on land only), the JJAS precipitation rates are increased by about 3.3 mm day$^{-1}$ (Fig. 8a). These values are quite a bit larger than the standard deviation of the mean simulated climate (which varies between 0.1 and 0.5 mm day$^{-1}$ in this region; see Fig. 8b). They are therefore statiscally significant, following a Student's t-test (not shown). The biggest changes are found west of Lake Chad (+3.8 mm day$^{-1}$ compared to +2.8 mm day$^{-1}$ east of Lake Chad) since this area is closer to the ocean, that is, to the source of water vapor. Moreover, the northern limit of rainfall, with rates larger than 1 mm day$^{-1}$ (which we attribute to the monsoon), is shifted northward by 2° compared to ctrl. Despite this increased moisture, the simulated change in annual precipitation−evapotranspiration ($P - E$) is insufficient to grow steppelike vegetation north of ~18°N, as discussed in Texier et al. (1997), who asynchronously coupled the LMD AGCM to a model that computes a biome distribution in equilibrium with the simulated climate (BIOME1; Prentice et al. 1992). In the southern part of the ITCZ (from 5° to 10°N) the mean zonal increase in rainfall is still significant but not as large as farther north (~1 mm day$^{-1}$).

In Asia the position of the maximum rainfall is not only extended but also slightly shifted farther inland, increasing the precipitation rates by 1.7 mm day$^{-1}$ over Tibet (averaged from 20° to 30°N, and 70° to 110°E) in JJAS, which is statistically significant. This migration induces significantly drier-than-present conditions in southern India and Indochina (−1.8 mm day$^{-1}$), while in Indonesia rainfall is increased by about 1.5 mm day$^{-1}$, and is associated with a northwestward movement of the main large-scale low-level convergence zone as displayed Fig. 9a. Joint displacements of the main convergent cell and of areas of maximum rains have already been observed and discussed in simulations with another version of the LMD model (de Noblet et al. 1996a).

These results are consistent with the ones obtained within the PMIP project (Joussaume et al. 1999).

### c. *The 6-kyr-BP simulated climate forced by both orbital configuration and changes in SST*

Compared to the present-day simulated climate, the pattern of change in rainfall (Fig. 8c), when both 6-kyr-BP orbital conditions and SST changes are prescribed, resembles the one obtained when the change in orbital forcing is considered alone (expt OF). The main difference with OF regards the intensity of the changes. In the northern branch of the ITCZ, rainfall is increased by about the same amount as in OF (~3.3 mm day$^{-1}$), but the differences are this time larger east of Lake Chad (+3.6 mm day$^{-1}$ compared to +2.8 mm day$^{-1}$ in OF). In the southern branch of the ITCZ (from 5° to 10°N) there is a rather large area of reduced precipitation (−0.3 mm day$^{-1}$, averaged from 5° to 10°N, 20°W to 40°E, over land only). These changes highlight the narrowing of the ITCZ in OFSST compared to both OF and Ctrl.

The increased rates over the Tibet, and the decreased rates over India, Indochina, and China, are of slightly lesser magnitude in OFSST than in OF (±1.3 mm day$^{-1}$ compared to ±1.7 mm day$^{-1}$), but differences are not significant. In Indonesia and in the regions located north of the Indian Ocean (west of Indonesia), on the other hand, rainfall is more strongly (and significantly) increased than in OF, and the areas affected by this increase are far more extended.

Compared to both Ctrl and OF, the prescribed changes in SSTs cause sea level pressure (SLP) to increase (colder water) west of the African coast and offshore of Arabia, and to decrease (warmer water) in the eastern part of the Oman Sea and in the Bay of Bengal. An increase (+2 hPa) is also observed in the west Pacific, east of China, although no SST change was prescribed there. This is the signature of the redistribution of air mass by meridional cells (of the ''Walker type'') within the northern Tropics and that can be identified looking at the changes in velocity potential at 200 hPa (Fig. 9b). Over land, the changes in SLP are similar to the ones obtained in response to orbital forcing alone. Compared to the control, the inland penetration of water vapor is increased at all latitudes from the equator to 18°N, as in OF (Figs. 7a,b). Compared to OF this inland penetration is decreased south of 12°N, despite the increased land–sea temperature and SLP contrast. Indeed, the strengthening of the oceanic high-pressure cells in the Atlantic reinforces the anticyclonic circulation, leading to stronger westward trade winds between the equator and 12°N. This pattern is consistent with the one presented by Wang et al. (1996), who studied the impact of a low-level atmospheric heating/cooling on the tropical circulation. Between 12° and 20°N, on the contrary, the increased land–sea contrast favors the return of the southward flow. This increased land–sea contrast, together with a ''piping'' of the flow (induced by the cooling of SSTs on both sides of the oceanic convergence zone), accelerates the onshore water vapor advection and favors a more eastward convergence. Thus,

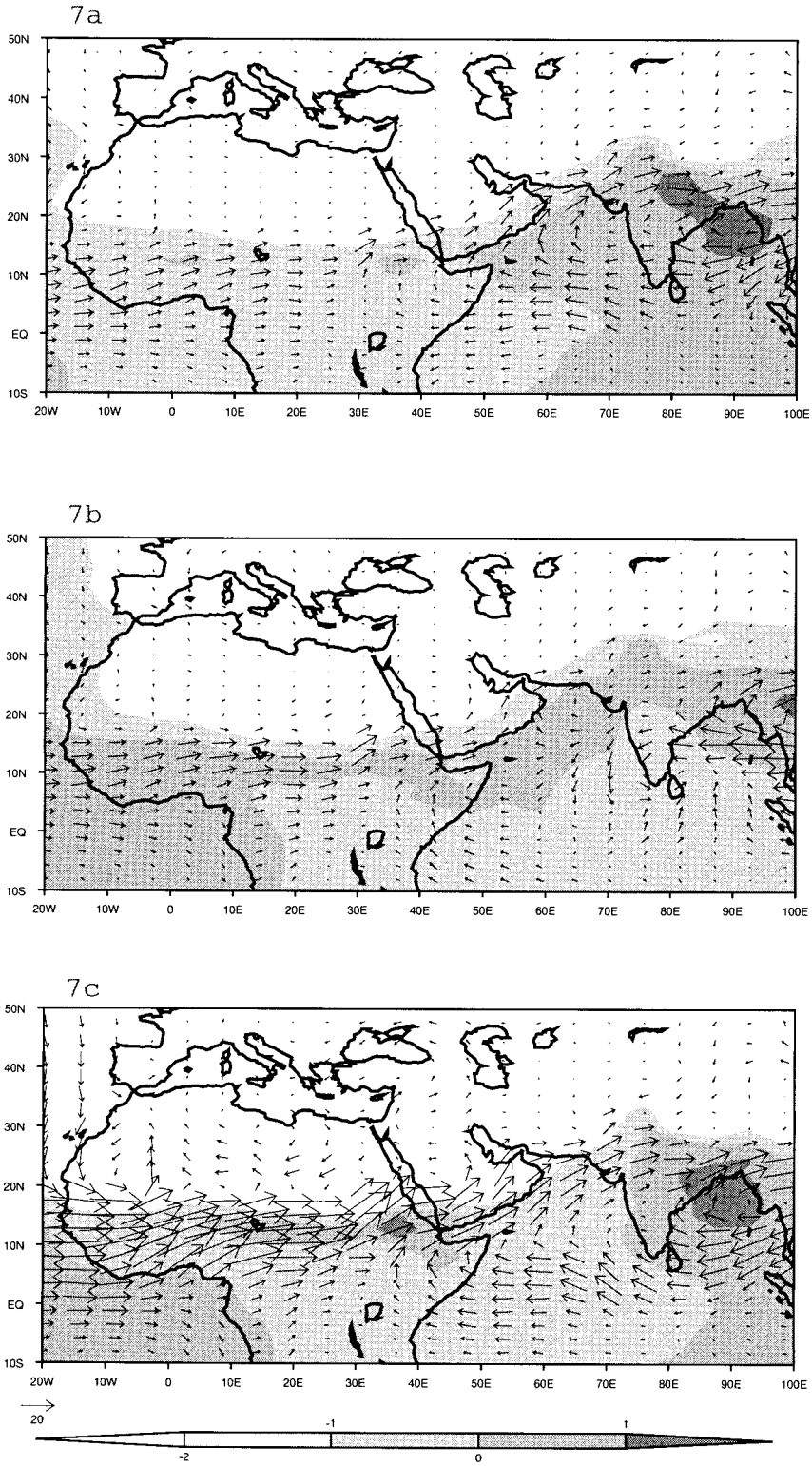


FIG. 7. Changes in the transport of latent heat ($10^8$ W $m^{-1}$) in the boundary layer in JJAS. Differences are between the simulated mid-Holocene climate and control. (a) The effect of orbital forcing alone (OF − Ctrl), (b) the combined effects of orbital forcing and SST changes (OFSST − Ctrl), and (c) the combined effects of orbital forcing and changes in the vegetation distribution (OFGS − Ctrl). Changes in SLP are shaded.

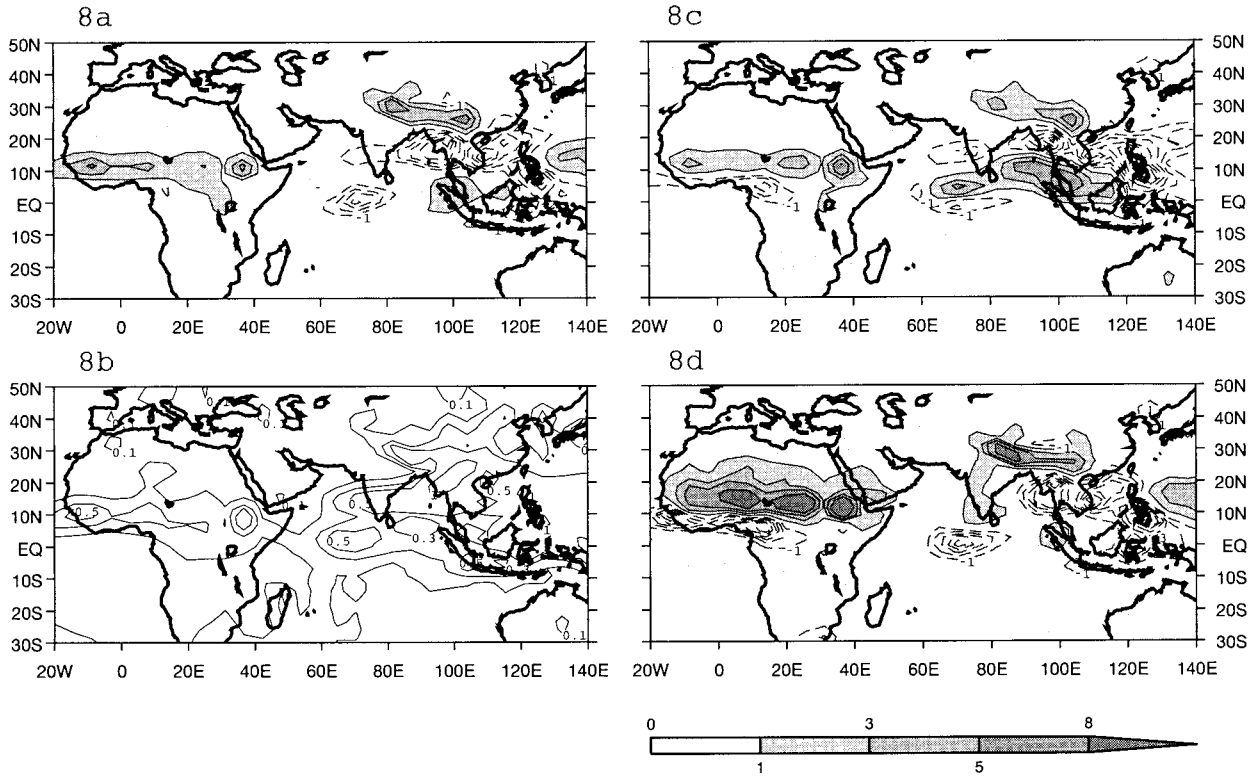


FIG. 8. Changes in the mean precipitation rates (mm day$^{-1}$), averaged from Jun to Sep. Differences are between the simulated mid-Holocene climate and present day. (a) The effect of orbital forcing alone (OF − Ctrl), (c) the combined effects of orbital forcing and SST changes (OFSST − Ctrl), and (d) the combined effects of orbital forcing and changes in the vegetation distribution (OFGS − Ctrl). Positive differences (i.e., increased rainfall during mid-Holocene) are shaded, and isolines are +1, +3, +5, and +8 mm day$^{-1}$. Negative contours are dashed and isolines are every 1 mm day$^{-1}$. (b) The mean standard deviation computed from the averaged control climate. Isolines are 0.1, 0.3, 0.5, and 1 mm day$^{-1}$.

compared to OF, the increase in rainfall in West Africa is reduced, whereas it is increased in the east.

For the Indian–Asian monsoon region, the simulated reduced land–sea contrast in OFSST compared to OF induces an increased east–west SLP gradient over the ocean, which reduces the inland penetration of moisture and forces convergence to occur at a more southward position, in the Bay of Bengal. Moreover, the prescription of warmer temperatures leads to larger rates of evaporation. The combination of both factors is the reason why precipitation is significantly increased in the oceanic regions.

### *d. The 6-kyr-BP simulated climate forced by both orbital configuration and changes in the distribution of vegetation*

The prescription of vegetation in the Sahara increases significantly the precipitation rates during the monsoon season by 6.7 mm day$^{-1}$ in the northern branch of the ITCZ (between 10° and 15°N), by 4.7 mm day$^{-1}$ between 15° and 20°N (the mean rate in Ctrl is 0.7 mm day$^{-1}$), and by 1 mm day$^{-1}$ between 20° and 30°N (the mean rate in Ctrl is 0.3 mm day$^{-1}$), the latter being the northernmost latitude of prescribed vegetation. We therefore, in OFGS, simulate a 10°-latitude northward extension of the northern limit (1 mm day$^{-1}$ isoline as a reference) of monsoon rains compared to present (Fig. 8d). In the western equatorial regions, on the contrary, rainfall is decreased by about 3 mm day$^{-1}$ and is the result of a 5°-latitude northward migration of the ITCZ in Africa (the maximum is located around 8°N in Ctrl and around 13°N in OFGS). Xue and Shukla (1996) and Bröstrom et al. (1998) reported similar results when they afforested the Sahel. OFGS is the only of our 6-kyr-BP experiments that shows a real migration of the ITCZ. In OF and OFSST the rainbelt (i.e., the regions, in northern Africa, where precipitation rates exceed 1 mm day$^{-1}$) extends farther north but the peak remains at its present-day position.

Monsoon rains are significantly enhanced over the Indian subcontinent, especially in the southern margin of the Tibetan plateau (+2.1 mm day$^{-1}$), and in southern India (+1.2 mm day$^{-1}$ compared to present), even though no vegetation change was prescribed in India. The large deepening of the thermal low over east Africa and Arabia enhances the low-level convergence (upper-level divergence) in these regions (Fig. 9c) and therefore

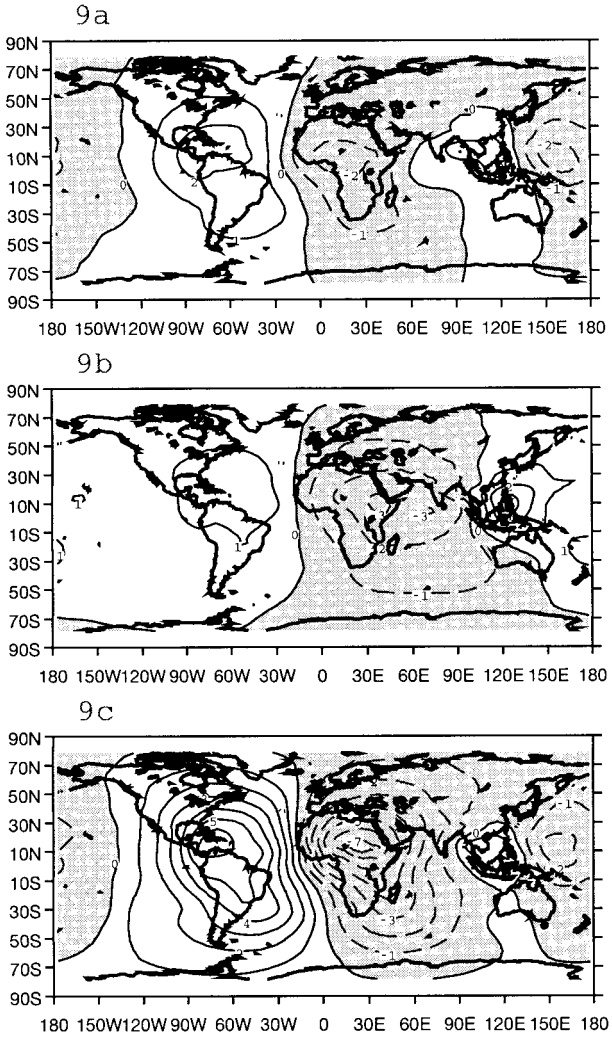


FIG. 9. Changes in the 200-hPa velocity potential ($\times 10^6$ m$^2$ s$^{-1}$) in JJAS. Differences are between the simulated mid-Holocene climate and present day. (a) The effect of orbital forcing alone (OF − Ctrl), (b) the combined effects of orbital forcing and SST changes (OFSST − Ctrl), and (c) the combined effects of orbital forcing and changes in the vegetation distribution (OFGS − Ctrl). Negative values (i.e., where the upper-level divergence is increased, or convergence decreased) are shaded. Negative contours are dashed. Isolines are every $10^6$ m$^2$ s$^{-1}$.

the southerly flow from the Indian Ocean into India, which contributes for a large amount to the simulated increase in precipitation (Fig. 8d). In addition the strong increase in water vapor advection coming from Africa (Fig. 7c) also participates in the enhanced rainfall.

In the Sahara, the imposed lower surface albedo (−13% from 15° to 30°N) induces quite warmer surface temperatures throughout the year (+1.5°C in spring and +3.8°C during the summer monsoon). Given that SSTs are not modified in OFGS compared to Ctrl and OF, the establishment of the continental thermal low is accompanied by land–sea temperature and SLP contrasts that are sharper than in both Ctrl and OF. Net solar heat flux at surface is increased in response to the change in albedo, and so is the downward infrared radiation due to the increased cloudiness in this region (atmospheric feedbacks to the prescribed changes in vegetation). Surface net radiation is then increased in OFGS between 15° and 30°N by 34 W m$^{-2}$ (annually), compared to Ctrl (the increase, compared to OF, is 32 W m$^{-2}$ and confirms that the change is mainly due to vegetation). This, together with increased surface roughness length (from 0.02 to 0.16 m), leads to larger fluxes of sensible heat (about 1.3 times larger in OFGS than in OF) north of 15°N, that is, where desert has been replaced by vegetation. The induced dry convection in spring favors the establishment of an onshore moisture flux between 15° and 20°N that is not simulated in Ctrl (Figs. 10a–c). Rainfall is then efficiently recycled by the prescribed vegetation. Interception loss is the dominant term in the total evapotranspiration rate during most of the rainy season (Figs. 10d–f). But when rainfall starts decreasing, transpiration takes over and becomes dominant, because it can pump up the moisture available for plants in the root zone. It is interesting to note that soil moisture, north of 15°N, is more abundant in Ctrl than in OFGS because it cannot be used for evaporation due to the absence of roots to transfer the water to the atmosphere (the resistance of a bare soil to evaporation increases sharply with decreasing soil moisture).

If we define the length of the monsoon season as the time during which water vapor advection (defined here as the difference between precipitation and evapotranspiration) is the dominant participant to precipitation, Fig. 11a shows that the monsoon season, between 5° and 15°N, starts at the exact same moment in both Ctrl and OFGS, but ends in August in Ctrl and in November in OFGS. This lenghtening of the monsoon season is mainly due to the presence of vegetation farther north that continues to pull the moisture flow until the end of August. A monsoon season, following the criteria defined above, also exists farther north in OFGS, although it is quite short (about 2 months between 15° and 20°N). The rather large amount of rain we simulate from May until October mainly comes from local evapotranspiration, plants being able to extract water in their root zone.

The very strong reinforcement of the summer monsoon circulation in northern Africa, in response to changing the land-surface cover, has also been found by Kutzbach et al. (1996), Claussen and Gayler (1997), and Bröstrom et al. (1998) for the mid-Holocene climate, and by Xue and Shukla (1996) for present day. They also found that the mechanism that starts the strengthening of the monsoon is partly driven by the change in albedo, as first described by Charney (1975). The other land-surface characteristics, such as roughness length or canopy resistance, also play an important role although our results do not permit us to separate their individual influence.

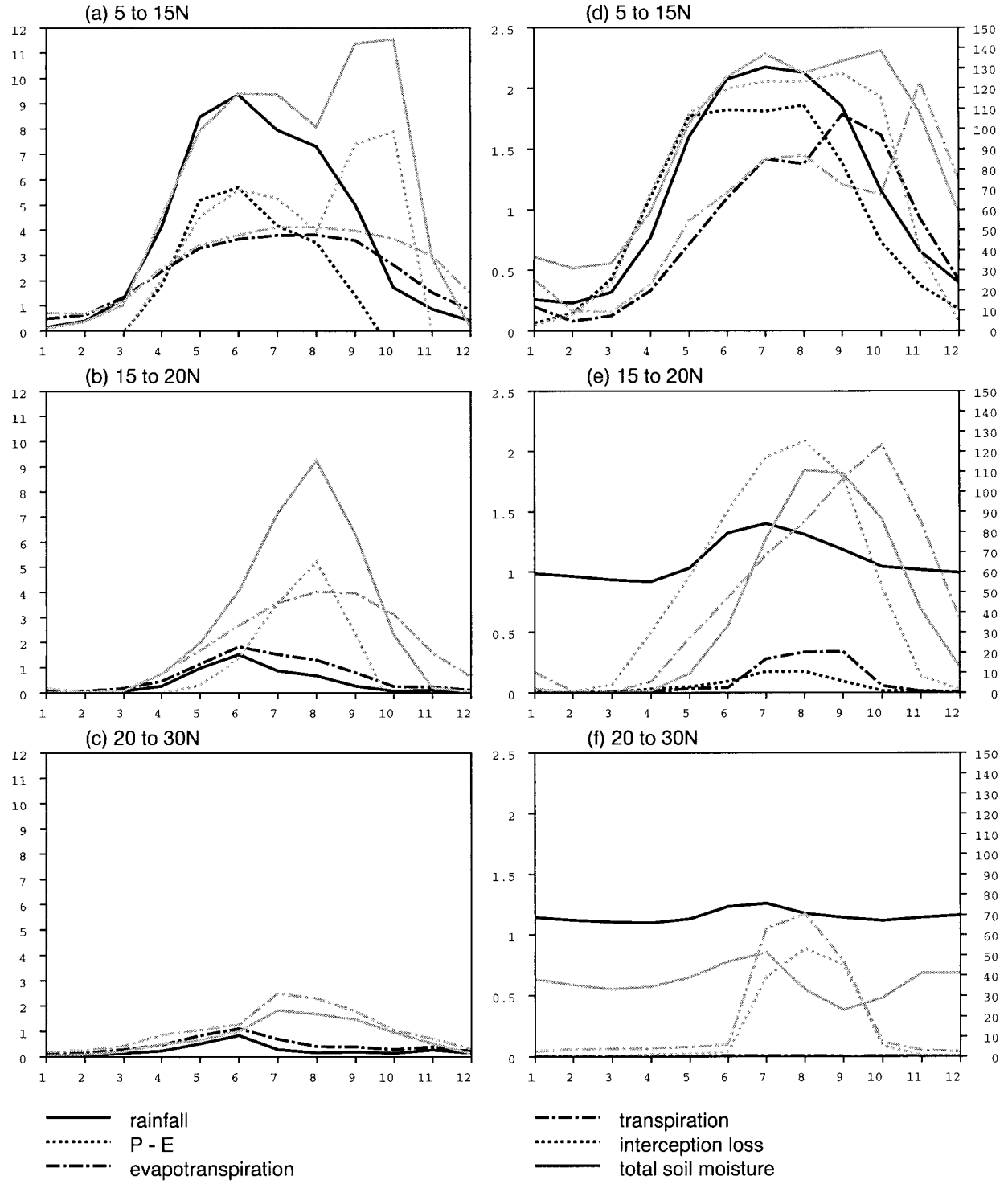


FIG. 10. Time evolution of mean quantities in northern Africa for Ctrl and OFGS. Averages are made longitudinally from 10°W to 30°E, and zonally from 5° to 15°N (a) and (d), 15° to 20°N (b) and (e), and 20° to 30°N (c) and (f). (left) The evolution of rainfall (plain lines), evapotranspiration (dashed–dotted lines), and difference between precipitation and evapotranspiration ($P - E$; dotted lines); (right) the evolution of total soil moisture in the root zone (plain lines), transpiration (dashed–dotted lines), and interception loss (dotted lines). The present-day simulation is represented using black lines, while OFGS is represented using gray lines.

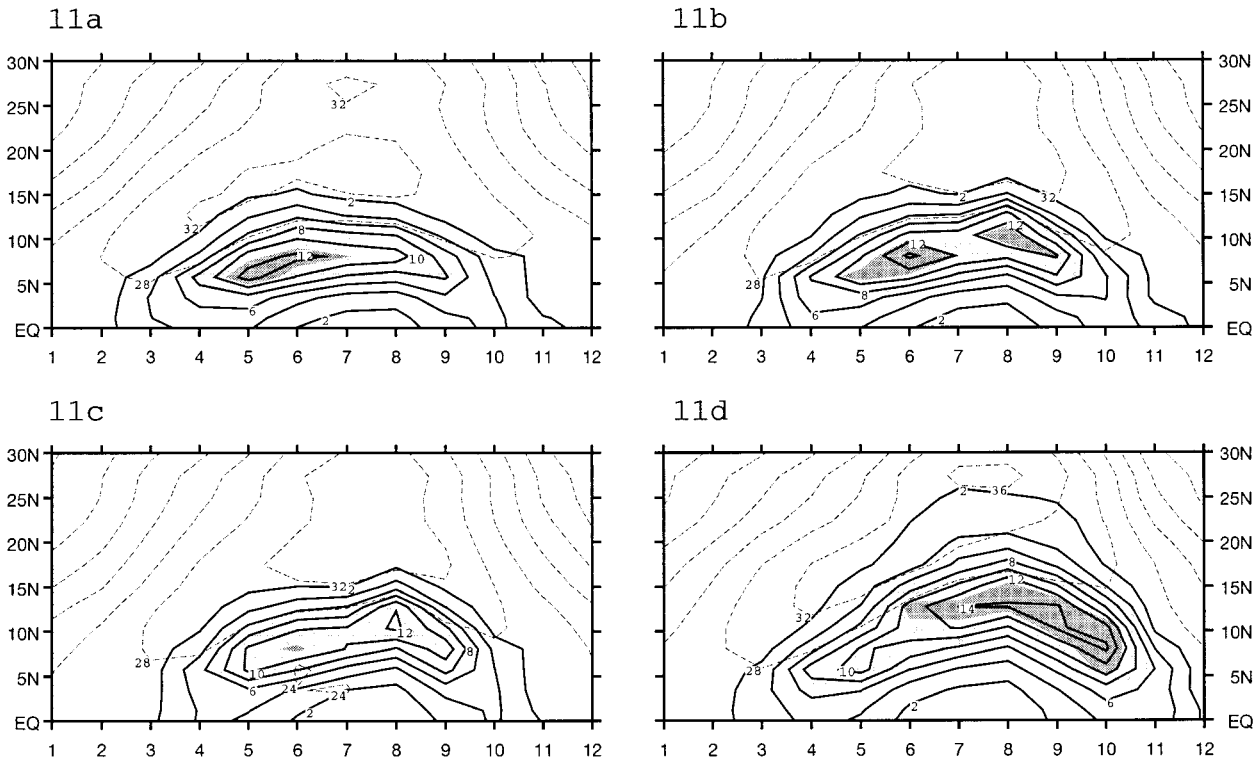


FIG. 11. Time evolution of precipitation (mm day$^{-1}$, solid line) and surface air temperature (°C, dashed line), zonally averaged over Africa (10°W–30°E) and plotted as a function of latitude. The shaded values represent the latitudes where, and the time when, the latent heat transport dominates the local recyling (i.e., $P - E >$ evapotranspiration) in the rainfall term. (a) The simulated present-day climate, (b) the orbitally induced mid-Holocene climate (OF), (c) the mid-Holocene climate simulated in response to both orbital and SST forcing (OFSST), and (d) the mid-Holocene climate simulated in response to both orbital and vegetation forcing (OFGS). Isolines are every 2 mm day$^{-1}$ for precipitation and every 4°C for temperature.

## 4. Mechanisms of monsoon changes over Africa

The results presented above show that both changes in SST (OFSST) and vegetation (OFGS) enhance the JJAS monsoon flow and precipitation in northern Africa compared to orbital forcing alone (OF). The northward penetration of the monsoon rains is well depicted in Fig. 11 where the zonal distribution of rainfall is plotted as a function of time, together with the surface temperature for all simulations. The northernmost (in July–August) extension of the ITCZ (2 mm day$^{-1}$ isoline) is located immediately to the south of the temperature maximum, which depicts the position of the minimum of the continental thermal low. Braconnot et al. (1997, manuscript submitted to *Global Planet. Change*) have already demonstrated that this feature is shared by all models in the international PMIP project, whatever the time period is (present, 6 and 21 kyr BP). They have moreover showed that there is a countergradient between precipitation and temperature to the north of the maximum of the ITCZ. The shape of the temperature gradient is a good indicator of how far north the monsoon flow penetrates in Africa. The change in orbital forcing prescribed in OF increases incident solar radiation and thereby soil temperature, and also displaces a few degrees (~2°) farther north the region of maximum temperature (Fig. 11b). This explains why the ITCZ is extending farther north in OF than in ctrl. However the simulated warming is not sufficient to move the location of the rainfall maximum farther north. There is no modification of the temperature distribution over land north of 8°N in OFSST compared to OF; this is probably the reason why the shape of the rainbelt in that region does not change (Fig. 11c). Differences in rainfall intensity between these two simulations therefore only arise from differences in water vapor advection south of 10°N (Fig. 7). In OFGS the large change in surface albedo has an impact on temperature, the maximum of which is shifted to the north. It is partly responsible for the northard migration of the ITCZ compared to Ctrl, OF, and OFSST (Fig. 11d), other factors being changes in latent and sensible heat fluxes via increased roughness length and decreased resistances to evapotranspiration (see section 3d).

Differences in the intensity and width of the monsoon rainbelt in our 6-kyr-BP simulations result from interactions between deep convection and the low-level moisture supply through water vapor advection and surface evapotranspiration. Latent heat released to the atmosphere, through condensation, helps increase the up-

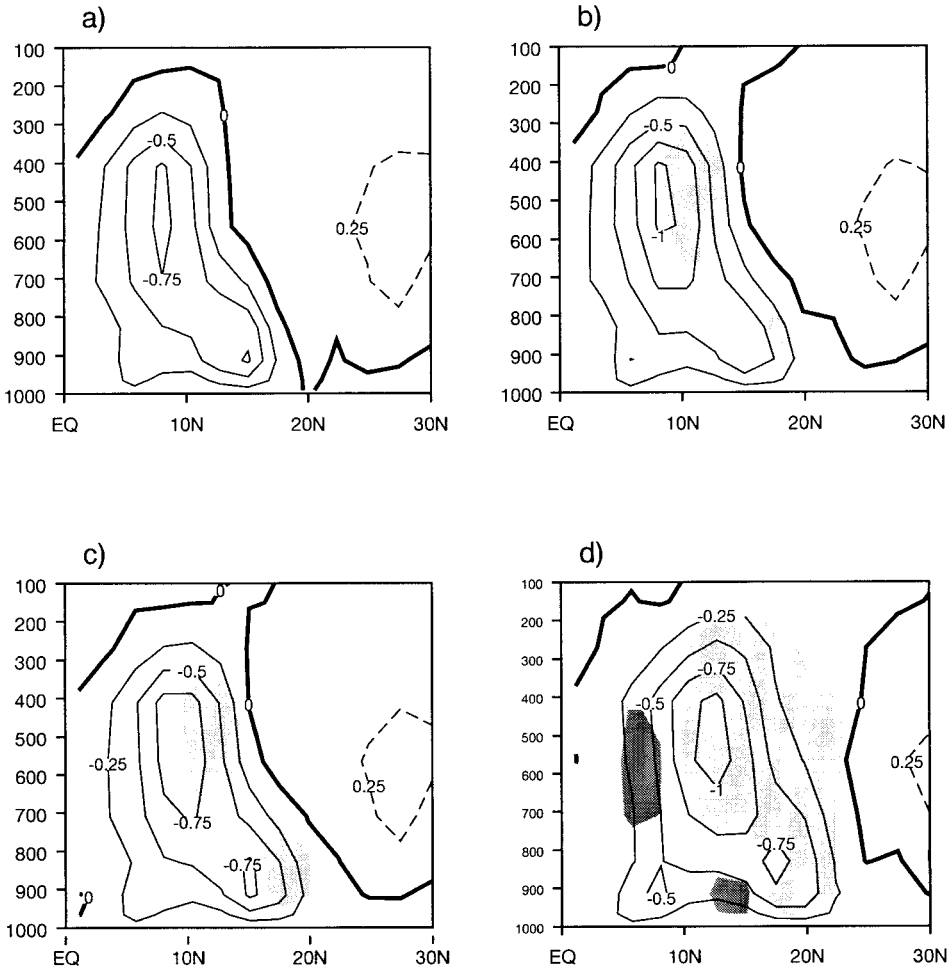


FIG. 12. Vertical velocity ($10^{-3}$ hPa $s^{-1}$) plotted as a function of latitude and altitude, zonally averaged over Africa (10°W–30°E) for JJAS. (a) The simulated present-day climate, (b) the orbitally induced mid-Holocene climate (OF), (c) the mid-Holocene climate simulated in response to both orbital and SST forcing (OFSST), and (d) the mid-Holocene climate simulated in response to both orbital and vegetation forcing (OFGS). Negative values (i.e., ascending motion) are plotted using solid lines, and positive values (i.e., subsidence) using dashed lines. Isolines are every $0.25 \times 10^{-3}$ hPa $s^{-1}$. Light shading corresponds to regions where the upward motion is increased; dark shading corresponds to regions where the upward motion is decreased.

ward motion and sustain low-level convergence. For all simulations, vertical velocity, zonally averaged between 10°W and 30°E from June to September, is plotted Fig. 12. Negative values correspond to upward motion and therefore highlight the location and latitudinal extension of the ITCZ. In the control, the core of the simulated ITCZ is located at 8°N where the upward vertical velocity is the largest, with the maximum ($>0.75 \times 10^{-3}$ hPa $s^{-1}$) located between 600 and 500 hPa (Fig. 12a). Large-scale subsidence (positive values of vertical velocity) are found on top of the vertical ascent at the latitudes of the ITCZ, and at all levels north of about 18°N. A convective area is also simulated at 15°N but is quite shallow and corresponds to the location of maximum temperature. Sensible heat flux, which only warms up the low atmosphere, triggers this convection. However, the increased convection is not accompanied by rainfall, since the latent heat flux is rather weak and there is no more water vapor advection at this latitude. In OF, in response to warmer land and increased advection, the convection becomes deeper (values larger than $10^{-3}$ hPa $s^{-1}$ being found from 600 to 400 hPa; Fig. 12b). The vertical velocity is enhanced at all levels north of the present-day ascent. The velocity patterns confirm that the ITCZ is expanded northward, but that the location of maximum intensity remains the same. In OFSST, the low-level moisture convergence occurs in a narrower latitudinal band than in OF, due to the prescription of colder SSTs on both sides of the ITCZ. North of 10°N, the upward vertical velocity is slightly

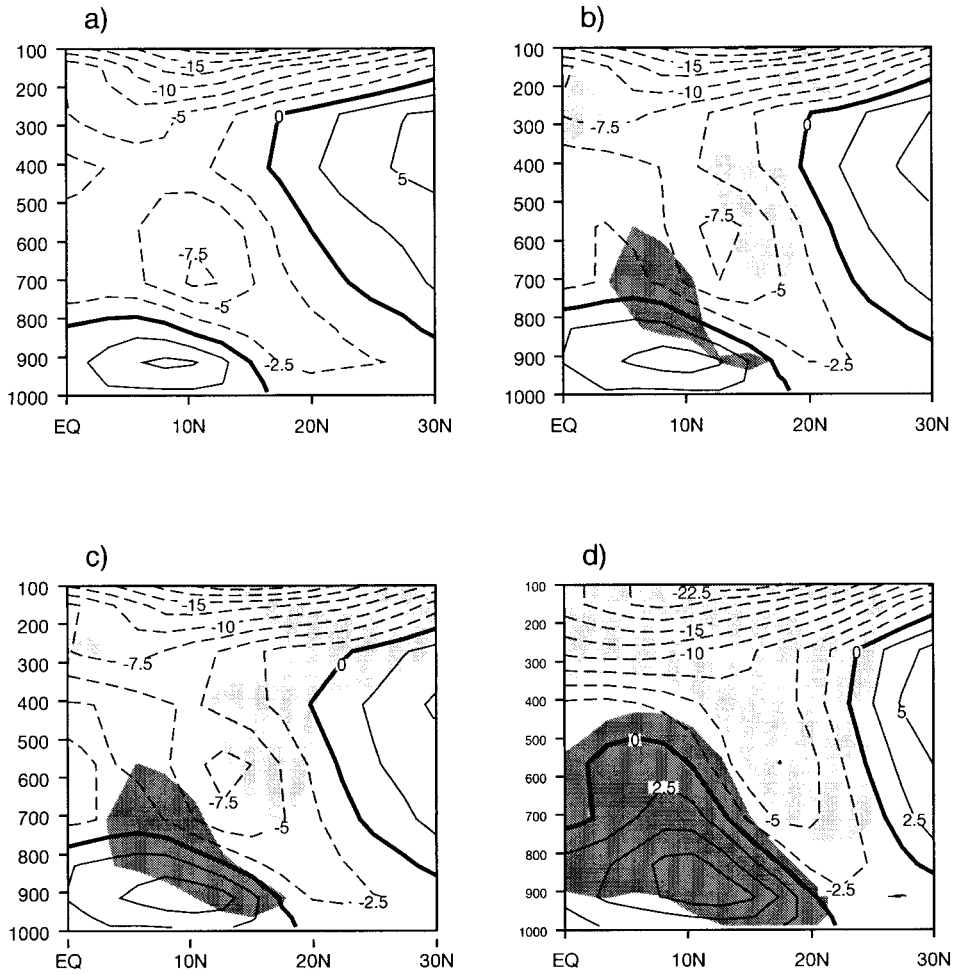


FIG. 13. Zonal wind (m $s^{-1}$) plotted as a function of latitude and altitude, zonally averaged over Africa (10°W–30°E) for JJAS. (a) The simulated present-day climate, (b) the orbitally induced mid-Holocene climate (OF), (c) the mid-Holocene climate simulated in response to both orbital and SST forcing (OFSST), and (d) the mid-Holocene climate simulated in response to both orbital and vegetation forcing (OFGS). Negative values (i.e., easterly wind) are dashed. Regions of increased easterly wind are lightly shaded while regions of decreased easterly wind are heavily shaded. Isolines are every 2.5 m $s^{-1}$.

enhanced (Fig. 12c), especially around 18°N. However, this brings no change in rainfall since this region corresponds to the limit of water vapor advection. South of 10°N upward motion is reduced together with precipitation. In contrast to the situation in OFSST, inclusion of vegetation in the Sahara strongly reinforces convection. Large-scale subsidence in OFGS is then confined to southern tropical latitudes and tropical regions located north of 22°N (Fig. 12d). The location of maximum velocity is displaced to the north, following the migration of the ITCZ. Its magnitude around 800 hPa is weaker than in OF but increased at higher levels because this is where more latent heat is released. This is due to the large impact that the change in vegetation north of 10°N has on surface heating and the hydrological cycle. The increased evapotranspiration rate, north of 15°N (see section 3d), not only contributes to increase the rainfall rates, but is also partly responsible for the larger amount of water vapor advected from the ocean by means of a dynamical trough created by the increased upward motion. In OFGS, the local Hadley cell is more efficient in exporting heat toward the Southern Hemisphere.

These changes in convection are accompanied by modifications of the African easterly jet (AEJ). Zonal winds, longitudinally averaged between 10°W and 30°E for JJAS, show that the core of the AEJ is located between 700 and 600 hPA at 11°N in our control simulation (Fig. 13a). The tropical easterly jet (TEJ) is found at 100 hPa (Dümenil and Bauer 1998). It gets stronger in response to all the applied forcings since they all induce a reinforcement of the Asian monsoon, with a maximum in OFGS (Figs. 13a–d). The behavior of the AEJ is more complex. In OF and OFSST, it is increased

and shifted slightly upward and northward (Figs. 13b,c), following the changes in vertical velocity. In OFGS, the structure of the jet is altered with a weakening and northward shift at 700 hPa and a strong enhancement at higher levels where it merges with the TEJ (Fig. 13d). These modifications of the jet are related to changes in the thermal structure of the atmosphere. The larger latent heat released in the ITCZ warms the atmospheric column between 700 and 400 hPa. At the same time the surface warming and the associated increase in sensible heating at low levels north of 18°N, together with a slightly increased subsidence over the northern part of the desert, warms the atmosphere in that region by a larger amount. The meridional temperature gradient between the equator and the northern Tropics is then enhanced and not reduced as one would have expected from the latent heat release only, and the jet is accelerated. For a given pressure level, the largest temperature gradient occurs at higher levels in OFGS, which, in our model, explains why the jet core is higher. The enhancement of the African monsoon is then associated with an upward shift, deepening, and strengthening of the AEJ. Most papers dealing with changes in African monsoon (e.g. Xue and Shukla 1993, 1996; Diedhiou and Mahfouf 1996) report a decrease of the AEJ in response to increased monsoon rains. If we look at our results we see that, indeed, at the altitude of the present-day AEJ the wind is decreasing. But farther up the wind is increasing.

## 5. Conclusions

Changes in sea surface temperature and vegetation distribution enhance the response of both African and Asian monsoons to 6-kyr-BP orbital forcing.

Regarding the African monsoon, the cooling in the upwelling zones off the coast of Africa in OFSST induces a narrowing of the ITCZ compared to the response to orbital forcing alone, with strongly reduced precipitation rates to the south of the peak and slightly increased rates to the north (larger inland advection of water vapor north of 10°N). Prescription of vegetation in the Sahara in OFGS, in place of the present desert, on the contrary leads to a large widening of the ITCZ accompanied by a 5° northward displacement of the peak rainfall in Africa. As with SST changes, precipitation decreases south of the peak of the ITCZ and increases to the north, but the magnitude of these differences is quite larger. This feature is not surprising since changing vegetation cover means modifying all land-surface characteristics (e.g., albedo, roughness length, resistances to evapotranspiration) and, therefore, the water and energy budgets. Moreover, the vegetation is more efficient in recycling rainfall through evapotranspiration. The larger release of latent heat in the atmospheric column during condensation helps maintain the convection and thereby an onshore moisture flow. The monsoon season is then lengthened in OFGS, in its present-day location (5°–15°N): it indeed continues through autumn (until the end of November), while in all other 6-kyr-BP experiments (OF and OFSST) the inland flow of the monsoon stops around mid-September (and at the end of August in Ctrl). We have moreover showed that, north of 15°N, a monsoon season does exist when we afforest the Sahara, while there is almost no rainfall in all other simulations. We have not seen any change in the date of the monsoon onset.

Regarding the Asian monsoon, cooling of the ocean in the eastern part of the Arabian Sea in OFSST has reduced the strength of the southwesterly flow and therefore the precipitation rates in India compared to the response to orbital forcing alone. The warming of the Bay of Bengal and the South China Sea, on the contrary, has strongly increased monsoon rains in Indonesia, southeast China, and over the oceanic regions. This is due to the decreased land–sea contrast and the increased evaporation rates over sea. In OFGS, even though no vegetation change was prescribed in Asia, rainfall is increased in India in response to 1) an increased southward flow coming from the Indian Ocean and responding to the enhancement of the large-scale convergent flow in East Africa, Arabia, and India; and 2) a slightly stronger eastward flow of moisture coming from Africa.

Bröstrom et al. (1998) have also studied the response of the African monsoon to a greening of the Sahara. Their forcings and results are quite comparable to ours. Indeed, both models show that the large change in rainfall simulated in Africa is in closer agreement with land-surface proxy data (pollen and lake levels; Jolly et al. 1998; Yu and Harrison 1996), when compared to orbital forcing alone. But interestingly, in none of the models is this increased precipitation (compared to Ctrl) sufficient to maintain the vegetation as it is prescribed. Claussen and Gayler (1997) and de Noblet et al. (1999, manuscript submitted to *Climate Dyn.*; starting from the experiment OFGS presented in this paper) have even shown that if the AGCM is asynchronously coupled to a biome model, the equilibrium mid-Holocene climate–vegetation reached when starting with a green Sahara, although much greener than today, is still desertic in large parts of the Sahara. These results imply that either the extent of vegetation we have prescribed is overestimated, or that it can only be sustained if all other boundary conditions, which have been fixed as for present-day (e.g., global SSTs, extent of inland water, etc.), are changed simultaneously. The latter point certainly needs further investigation.

We may note that the Bröstrom et al. (1998) experiment, as well as ours, found the existence of a monsoon signal between 15° and 25°N when the desert is being afforested. It would be interesting to know if they also found a lengthening of the monsoon season in the location of the present-day ITCZ because the question of whether a change of vegetation can or cannot induce a modification in the timing of the African monsoon (which would certainly be of help to the understanding

of present-day monsoon variability and sensitivity to anthropogenic influence) remains an open one. Indeed, in the real world, available observations do not provide clear evidence of changes in the length of the Sahelian rainy season with the desertification observed in this region during the last decades (Dennett et al. 1985).

We have shown that prescribed changes in sea surface temperatures (in OFSST) slightly enhance the African rainfall in the eastern part of the Sahel but do not push its northern limit farther north. This small change in rainfall rates may result from the fact that we have neglected one important aspect of oceans: their thermal inertia. Indeed, because of its delayed response to increased insolation, oceans are cooler than land during springtime, thereby increasing the land–sea pressure gradient and thus the inland advection of moisture. These midseason mechanisms could not be accounted for in OFSST due to the lack of data-inferred SST during late spring. Some experiments have quantified the impact of mid-Holocene insolation changes on SSTs, by coupling an AGCM to either a slab ocean (Mitchell et al. 1988; Kutzbach and Gallimore 1988) or an oceanic GCM (Kutzbach and Liu 1997; Hewitt and Mitchell 1998; Braconnot et al. 1997, manuscript submitted to *Global Planet. Change*). These experiments have shown that the ocean–land thermal contrast during midseasons was indeed stronger than now 6 kyr BP, and helped increase monsoon rains farther north in northern Africa.

*Acknowledgments.* We warmly thank Colin Prentice and Dominique Jolly for helping in defining the biome distribution used in the 6-kyr-BP ''green Sahara'' experiment. We also thank Hartmut Schulz and Nejib Kallel for helpful discussions on the definition of the boundary conditions used in the 6-kyr-BP experiment with prescribed changes in sea surface temperatures. We are grateful to Sylvie Joussaume and Sandy Harrison for the constructive discussions, which helped improve the first version of the manuscript. The remarks of an anonymous reviewer helped correct mistakes that were present in the first submitted version of the paper. The simulations were performed at the Laboratoire des Sciences du Climat et de l'Environnement and sponsored by EEC, under Contract ENV4-CT95-0075.

## REFERENCES

Berger, A., 1978: Long-term variation of daily insolation and quaternary climatic changes. *J. Atmos. Sci.,* **35,** 2362–2367.

Bröstrom, A., M. Coe, S. P. Harrison, R. Gallimore, J. E. Kutzbach, J. Foley, I. C. Prentice, and P. Behling, 1998: Land-surface processes and paleomonsoons in northern Africa. *Geophys. Res. Lett.,* **25** (19), 3615–3618.

Cadet, D. L., and G. Reverdin, 1981: Water vapour transport over the Indian Ocean during the summer 1975. *Tellus,* **33,** 476–487.

——, and S. H. Houston, 1984: Precipitable water over Africa and the Eastern/Central Atlantic Ocean during the 1979 summer. *J. Meteor. Soc. Japan,* **62,** 761–774.

Charney, J. G., 1975: Dynamics of deserts and drought in the Sahel. *Quart. J. Roy. Meteor. Soc.,* **101** (428), 193–202.

Claussen, M., and V. Gayler, 1997: The greening of the Sahara during the mid-Holocene: Results of an interactive atmosphere-biome model. *Global Ecol. Biogeogr. Lett.,* **6,** 369–377.

Coe, M. T., and G. B. Bonan, 1997: Feedbacks between climate and surface water in northern Africa during the middle Holocene. *J. Geophys. Res.,* **102** (D10), 11 087–11 101.

COHMAP, 1988: Climatic changes of the last 18,000 years: Observations and model simulations. *Science,* **241,** 1043–1052.

Dennett, M. D., J. Elston, and J. A. Rodgers, 1985: A reappraised rainfall trend in the Sahel. *J. Climatol.,* **5,** 353–361.

de Noblet, N., P. Braconnot, S. Joussaume, and V. Masson, 1996a: Sensitivity of simulated Asian and African summer monsoons to orbital induced variations in insolation 126, 115 and 6 kBP. *Climate Dyn.,* **12,** 589–603.

——, I. C. Prentice, S. Joussaume, D. Texier, A. Botta, and A. Haxeltine, 1996b: Possible role of atmosphere-biosphere interactions in triggering the last glaciation. *Geophys. Res. Lett.,* **23** (22), 3191–3194.

Diedhiou, A., and J. F. Mahfouf, 1996: Comparative influence of land and sea surfaces on the Sahelian drought: A numerical study. *Ann. Geofis.,* **14,** 115–130.

Druyan, L. M, and R. D. Koster, 1989: Sources of Sahel precipitation for simulated drought and rainy seasons. *J. Climate,* **2,** 1438–1446.

Ducoudré, N., K. Laval, and A. Perrier, 1993: SECHIBA, a new set of parameterizations of the hydrologic exchanges at the land–atmosphere Interface within the LMD atmospheric general circulation model. *J. Climate,* **6,** 248–273.

Dümenil, L., and H.-S. Bauer, 1998: The tropical easterly jet in a hierarchy of GCMs and in reanalyses. Max Planck Institute for Meteorology, Rep. ISSN 0937-1060, 45 pp. [Available from Max-Planck-Institut für Meteorologie, Bundesstrasse 55, 20146 Hamburg, Germany.]

Duplessy, J. C., 1982: Glacial to interglacial contrasts in the northern Indian Ocean. *Nature,* **295,** 494–498.

Fouquart, Y., and B. Bonnel, 1980: Computations of solar heating of the Earth's atmosphere: A new parameterization. *Beitr. Phys. Atmos.,* **53,** 35–62.

Gadgil, S., A. Guruprasad, D. R. Sikka, and D. K. Paul, 1992: Intraseasonal variation and simulation of the Indian summer monsoon. Simulation of interannual and intraseasonal monsoon variability. Rep. WCRP-68, World Meteorological Organization, 185 pp.

Hall, N. M. J., and P. J. Valdes, 1997: A GCM simulation of the climate 6000 years ago. *J. Climate,* **10,** 3–17.

Harzallah, A., and R. Sadourny, 1995: Internal versus SST-forced atmospheric variability as simulated by an atmospheric general circulation model. *J. Climate,* **8,** 474–498.

Hewitt, C. D., and J. F. B. Mitchell, 1996: GCM simulations of the climate of 6 kyr BP: Mean changes and interdecadal variability. *J. Climate,* **9,** 3505–3529.

——, and ——, 1998: A fully coupled GCM simulation of the mid Holocene. *Geophys. Res. Lett.,* **25,** 361–364.

Jarvis, D. I., 1993: Pollen evidence of changing Holocene monsoon climate in Sichuan Province, China. *Quat. Res.,* **39,** 325–337.

Jolly, D., and Coauthors, 1998: Biome reconstruction from pollen and plant macrofossil data for Africa and the Arabian peninsula at 0 and 6 ka. *J. Biogeogr.,* **25,** 1007–1028.

Joussaume, S., and K. Taylor, 1995: Status of the Paleoclimate Modelling Intercomparison Project (PMIP). *Proc. First Int. AMIP Scientific Conf.,* Monterey, CA, PCMDI, 425–430.

——, and P. Braconnot, 1997: Sensitivity of paleoclimate simulation results to season definition. *J. Geophys. Res.,* **102** (D2), 1943–1956.

——, R. Sadourny, and C. Vignal, 1986: Origin of precipitating water in a numerical simulation of the July climate. *Ocean–Air Interact.,* **1,** 43–56.

——, and Coauthors, 1999: Monsoon changes/regional climates for 6000 years ago: Results of 18 simulations from the Palaeoclimate

Modelling Intercomparison Project (PMIP). *Geophys. Res. Lett.*, **26,** 859–862.
Ju, J., and J. Slingo, 1995: The Asian summer monsoon and ENSO. *Quart. J. Roy. Meteor. Soc.*, **121,** 1133–1168.
Kallel, N., M. Paterne, L. Labeyrie, J.-C. Duplessy, and M. Arnold, 1997: Temperature and salinity records of the Tyrrhenian Sea during the last 18,000 years. *Palaeogeogr. Palaeoclimatol. Palaeoecol.*, **135,** 97–108.
Kuo, H. L., 1965: On the formation and intensification of tropical cyclones through latent heat release by cumulus convection. *J. Atmos. Sci.*, **22,** 40–63.
Kutzbach, J. E., and P. J. Guetter, 1986: The influence of changing orbital parameters and surface boundary conditions on climate simulations for the past 18 000 years. *J. Atmos. Sci.*, **43,** 1726–1759.
——, and R. G. Gallimore, 1988: Sensitivity of a coupled atmosphere/mixed layer ocean model to changes in orbital forcing at 9000 years BP. *J. Geophys. Res.*, **93** (D1), 803–821.
——, and Z. Liu, 1997: Response of the African monsoon to orbital forcing and ocean feedbacks in the middle Holocene. *Science*, **278,** 440–443.
——, P. J. Guetter, P. J. Behling, and R. Selin, 1993: Simulated climatic changes: Results of the COHMAP climate-model experiments. *Global Climates Since the Last Glacial Maximum*, H. E. Wright Jr. et al., Eds., University of Minnesota Press, 24–93.
——, G. Bonan, J. Foley, and S. P. Harrison, 1996: Vegetation and soil feedbacks on the response of the African monsoon to orbital forcing in the early to middle Holocene. *Nature*, **384,** 623–626.
Lamb, P. J., and R. A. Peppler, 1992: Further case studies of tropical Atlantic surface atmospheric and oceanic patterns associated with sub-Saharan drought. *J. Climate*, **5,** 476–488.
Legates, D. R., and C. J. Willmott, 1990: Mean seasonal and spatial variability in gauge-corrected precipitation. *Int. J. Climatol.*, **10,** 111–127.
Liao, X., F. A. Street-Perrott, and J. F. B. Mitchell, 1994: GCM experiments with different cloud parameterization: Comparisons with palaeoclimatic reconstructions for 6000 years BP. *Palaeoclim. Data Modell.*, **1,** 99–123.
Manabe, S., and R. F. Strickler, 1964: Thermal equilibrium of the atmosphere with a convective adjustment. *J. Atmos. Sci.*, **21,** 361–385.
Masson, V., and S. Joussaume, 1997: Energetics of mid-Holocene atmospheric circulation change in boreal summer from large-scale to monsoon areas: A study with two versions of the LMD AGCM. *J. Climate*, **10,** 2888–2903.
Mitchell, J. F. B., N. S. Grahame, and K. J. Needham, 1988: Climate simulations for 9000 years Before Present: Seasonal variations and effects of the Laurentide Ice Sheet. *J. Geophys. Res.*, **93** (D7), 8283–8303.
Morcrette, J. J., 1991: Radiation and cloud radiative properties in the ECMWF operational weather forecast model. *J. Geophys. Res.*, **96,** 9121–9132.
Morley, J. J., and B. A. Dworetzky, 1993: Holocene temperatures patterns in the south Atlantic, Southern, and Pacific Oceans. *Global Climates Since the Last Glacial Maximum*, H. E. Wright Jr. et al., Eds., University of Minnesota Press, 194–220.
Palmer, T. N., 1986: Influence of the Atlantic, Pacific and Indian oceans on Sahel rainfall. *Nature*, **322,** 251–253.
Petit-Maire, N., and N. Page, 1992: Remotes sensing and past climatic changes in tropical deserts: Example of the Sahara. *Episodes*, **15,** 113–117.
Prell, W. L., 1984a: A response to changing solar radiation. *Milankowitch and Climate, Part I*, A. Berger et al., Eds., D. Reidel, 349–366.
——, 1984b: Variation of monsoonal upwelling: A response to changing solar radiation. *Climate Processes and Climate Sensitivity*, J. Hansen and T. Takahashi, Eds., American Geophysical Union, 48–57.
——, and E. van Campo, 1986: Coherent response of Arabian Sea upwelling and pollen transport to the late quaternary monsoonal winds. *Nature*, **323,** 526–528.
——, and R. E. Marvil, 1990: Variability in upwelling fields in the northwestern Indian Ocean; 2. Data-model comparison at 9000 years BP. *Paleoceanography*, **5** (3), 447–457.
Prentice, I. C., W. Cramer, S. P. Harrison, R. Leemans, R. A. Monserud, and A. M. Solomon, 1992: A global biome model based on plant physiology and dominance, soil properties and climate. *J. Biogeogr.*, **19,** 117–134.
Raynaud, D., J. Jouzel, J. Barnola, J. Chappelaz, R. Delmas, and C. Lorius, 1993: The ice record of greenhouse gases. *Science*, **259,** 926–934
Reynolds, R. W., 1988: Real-time global sea surface temperature analysis. *J. Climate*, **1,** 75–86.
Roberts, N., and H. E. Wright Jr., 1993: Vegetational, lake-level, and climatic history of the near east and southwest Asia. *Global Climates Since the Last Glacial Maximum*, H. E. Wright Jr. et al., Eds., University of Minnesota Press, 194–220.
Ruddiman, W. F., and A. C. Mix, 1993: The north and equatorial Atlantic at 9000 and 6000 yr BP. *Global Climates Since the Last Glacial Maximum*, H. E. Wright Jr. et al., Eds., University of Minnesota Press, 194–220.
Sadourny, R., and K. Laval, 1984: January and July performance of the LMD general circulation model. *New Perspectives in Climate Modelling*, A. Berger and C. Nicolis, Eds., Elsevier, 173–198.
Schulz, H., 1995: Sea-surface temperature 9,000 years BP—Consequences of the early Holocene isolation maximum. Ph.D. thesis, University of Kiel.
Semazzi, F. H. M., B. Burns, N. H. Lin, and J. K. Schemm, 1996: A GCM study of the teleconnections between the continental climate of Africa and global sea surface temperature anomalies. *J. Climate*, **9,** 2480–2496.
Street, F. A., and A. T. Grove, 1976: Environmental and climatic implications of late quaternary lake-level fluctuations in Africa. *Nature*, **261,** 385–390.
Street-Perrott, F. A., and R. A. Perrott, 1993: Holocene vegetation, lake levels and climate of Africa. *Global Climates Since the Last Glacial Maximum*, H. E. Wright Jr. et al., Eds., University of Minnesota Press, 318–356.
——, J. F. B. Mitchell, D. S. Marchand, and J. S. Brunner, 1990: Milankovitch and albedo forcing of the tropical monsoons: A comparison of geological evidence and numerical simulations for 9000 yBP. *Trans. Roy. Soc. Edinburgh: Earth Sci.*, **81,** 407–427.
Sud, Y. C., J. Shukla, and Y. Mintz, 1988: Influence of land-surface roughness on atmospheric circulation and precipitation: A sensitivity study with a general circulation model. *J. Appl. Meteor.*, **27,** 1036–1054.
Swain, A. M., J. E. Kutzbach, and S. Hastenrath, 1983: Estimates of Holocene precipitation for Rajasthan, India, based on pollen and lake-level data. *Quat. Res.*, **19,** 1–17.
Texier, D., and Coauthors, 1997: Quantifying the role of biosphere-atmosphere feedbacks in climate change: A coupled model simulation for 6000 yr BP and comparison with palaeodata for northern Eurasia and northern Africa. *Climate Dyn.*, **13,** 865–882.
Van Campo, E., J. C. Duplessy, and M. Rossignol-Strick, 1982: Climate conditions deduced from a 150-kyr oxigen isotope-pollen record from the Arabian sea. *Nature*, **296,** 56–59.
Wang, T.-A., Y.-L. Lin, H. F. M. Semazzi, and G. S. Janowitz, 1996: Response of a stably stratified atmosphere to large-scale diabatic forcing with applications to wind patterns in Brazil and the Sahel. *J. Geophys. Res.*, **101** (D3), 7049–7073.
Winkler, M. G., and P. K. Wang, 1993: The late-quaternary vegetation and climate of China. *Global Climates Since the Last Glacial Maximum*, H. E. Wright Jr. et al., Eds., University of Minnesota Press, 221–264.
Xue, Y., and J. Shukla, 1993: A numerical experiment to study the

influence of changes in the land properties on Sahel climate. Part I: Desertification. *J. Climate*, **6,** 2232–2245.
——, and ——, 1996: The influence of land surface properties on Sahel climate. Part II: Afforestation. *J. Climate*, **9,** 3260–3275.
Yu, G., and S. P. Harrison, 1996: An evaluation of the simulated water balance of Eurasia and northern Africa at 6000 yr BP using lake status data. *Climate Dyn.*, **12** (11), 723–735.
——, I. C. Prentice, S. P. Harrison, and X. Sun, 1998: Pollen-based biome reconstructions for China at 0 and 6ka. *J. Biogeogr.*, **25,** 1055–1070.